COMPUTATION OF MASS TRANSFER FOR ROTATING SPIRAL MICROCHANNEL DISTILLATION

J Ortiz-Osorio, J M MacInnes, P J Jordan[†], G H Priestman and R W K Allen

Department of Chemical and Process Engineering, University of Sheffield, UK
[†]Department of Chemical and Process Engineering, University of Canterbury, NZ

Abstract: Performance prediction of microchannel distillation based on rotating spiral contacting is presented. Numerical computations of the flow and composition fields are carried out in the two-dimensional cross-section of the two-phase contacting flow using the Navier-Stokes and species equations simplified for the developed flow state. The approximation of a locally constant mass transfer rate of species is made and mass transfer coefficients for each phase are determined. Numerical predictions of the 'top' and 'bottom' composition for a micro distillation experiment reported elsewhere by the authors is found to be within 1% of the measured results. The procedure described can be utilised for the design of new devices based on rotating spiral contacting.

Keywords: microchannel, distillation, rotation, centrifugal, mass transfer coefficient

1. INTRODUCTION

MacInnes *et al*., (2008) demonstrated distillation using a rotating spiral microchannel in which centrifugal force is used to drive, segregate and organise the two contacting phases, i.e. the liquid and vapour. (See Figure 1). In order to produce distillation using this method a liquid feedstock is introduced to a 'contacting' spiral channel for which the temperature is arranged to increase with distance along the channel. The liquid flows outward along the channel and thus increases in temperature until eventually significant evaporation occurs. The evaporation increases the pressure near the end of the spiral channel driving the vapour phase back up the spiral counter to the liquid flow. This method contrasts with other published work where static microchannels with porous barriers between the phases (membranes) are used (Tonkovich *et al*., 2007; Tonkovich *et al*., 2008) and with the approach of Wootton and deMello (2005) using a carrier gas to promote separation. The present work introduces a computational approach for predicting the performance of contacting a rotating spiral microchannel. The computation is based on the solution of the governing equations for flow and species for the developed flow state using the approximation of a locally constant species mass transfer rate. Further it is assumed that the interface shape is entirely determined by balance of surface force and a Laplace pressure rise, so the interface is cylindrical and determined a priori. From the numerical solution one can compute the mass transfer coefficients and from these determine the bulk composition of each phase as a function of position along the spiral contacting channel. Thus, the product compositions can be predicted.

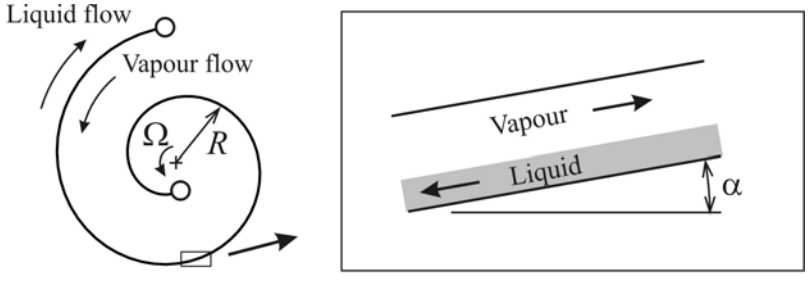

Fig. 1. Rotating spiral microchannel contactor; principle of operation (MacInnes *et al*., 2005).

2. COMPUTATIONAL APPROACH

Preliminary computations of the flow in the liquid phase were carried out by MacInnes *et al*. (2005) where the potential for mass transfer enhancement associated with secondary motions arising from Coriolis force on the liquid phase was noted. Here the computation is extended to include mass transfer interaction as well as flow in both phases and results are produced for comparison with measurements in the experimental distillation of MacInnes et al. (2008). The microchannel used in the experiment was fabricated by wet-etching glass with hydrofluoric acid (HF) resulting in a cross-section shape similar to that of a 'bowl' as shown in Figure (2). The microchannel has a width $W = 320\ \mu\text{m}$ and a depth of $H = 110\mu\text{m}$. The hydrocarbons utilised are wetting with a contact angle of 0^o so the interface can be considered as circular arc that is tangent to the wall surfaces. The interface between the fluids divides the domain into two regions, the liquid properties prevailing in one and the vapour properties in the other, with appropriate continuity conditions for the two phases at the interface surface.

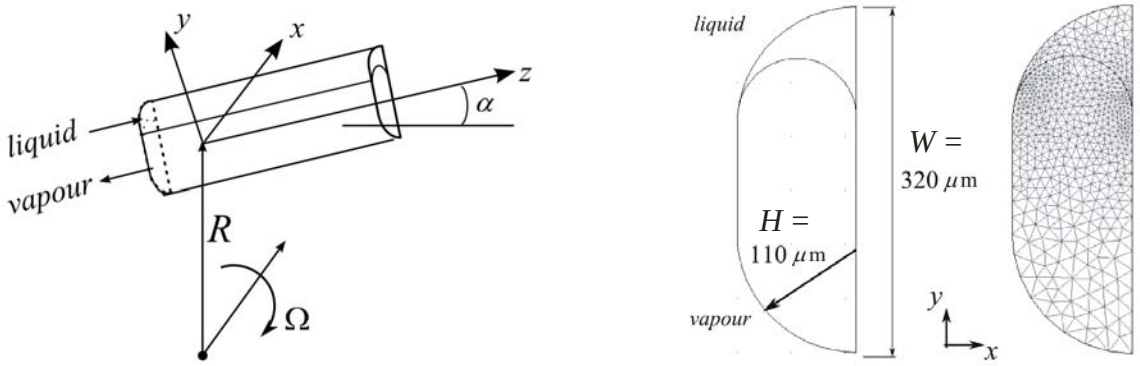

Fig. 2. Coordinate system and computational domain. R is the radial position of the centre of the channel, α is the local angle of inclination and Ω is the rotation vector.

2.1 The equation system

The momentum, continuity and species equations apply in the 2D section of the channel for developed flow. At this stage the energy equation is not solved, but instead the temperature field is assumed to match that required by the computed species field. Using the rotating coordinate system of Figure 2, the resulting equations for the velocity components (u, v, w) pressure (p) and the mole fraction of the least volatile species in a binary mixture (Y) are written:

x-momentum

$$\rho u\frac{\partial u}{\partial x}+\rho v\frac{\partial u}{\partial y}=-\frac{\partial p}{\partial x}+\mu\left(\frac{\partial^2 u}{\partial x^2}+\frac{\partial^2 u}{\partial y^2}\right) \tag{1}$$

y-momentum

$$\rho u\frac{\partial v}{\partial x}+\rho v\frac{\partial v}{\partial y}=-\frac{\partial p}{\partial y}+\mu\left(\frac{\partial^2 v}{\partial x^2}+\frac{\partial^2 v}{\partial y^2}\right)+2\rho\Omega w \tag{2}$$

z-momentum

$$\rho u\frac{\partial w}{\partial x}+\rho v\frac{\partial w}{\partial y}=-\frac{\mathrm{d}P_B}{\mathrm{d}z}+\mu\left(\frac{\partial^2 w}{\partial x^2}+\frac{\partial^2 w}{\partial y^2}\right)+\rho\Omega^2 R\sin\alpha-2\rho\Omega v \tag{3}$$

Continuity

$$\frac{\partial \rho u}{\partial x}+\frac{\partial \rho v}{\partial y}=0 \tag{4}$$

Species equation

$$nu\frac{\partial Y}{\partial x}+nv\frac{\partial Y}{\partial y}=-nw\frac{\mathrm{d}Y_B}{\mathrm{d}z}+nD\left(\frac{\partial^2 Y}{\partial x^2}+\frac{\partial^2 Y}{\partial y^2}\right) \tag{5}$$

n is the molar density, ρ the mass density, μ the viscosity, D the diffusivity; the centrifugal body force $\rho\Omega^2 R\sin\alpha$ brings in the angular velocity, Ω, and the spiral parameters: radius R and angle α. The body force in Eq. 3 is a constant in either phase since for the experimental design $R\sin\alpha = 0.00539$ m is constant. The final terms in Eqs. 2 and 3 are Coriolis force terms, with that in Eq. 2 producing secondary motions in the flow of each phase. Pressure gradient along the channel, dP_B/dz, is constant over the channel section for developed flow and its value together with a reference value for pressure must be supplied to close the equations. Similarly dY_B/dz in one of the phases and a reference value must be supplied to close the species equation. This corresponds indirectly to fixing the bulk mole fraction in each phase which is required to fix the particular conditions of mass transfer for the section. Eqs. 1 to 5 apply equally in each of the phases, differing simply in the values of the physical properties. The equations were solved numerically using COMSOL Multiphysics.

In addition to the usual no-slip and zero flux of species at wall boundaries, continuity conditions apply at the phase interface. The constraints for continuity of velocity, surface force components in *x*, *y* and *z* directions and flux conditions are given below. As mentioned, the interface shape is assumed to be precisely cylindrical with the consequence that the velocity must be constrained to be tangent to the interface (first of Eqs. 6). Also, computed pressure on the vapour side, p_V, is relative to the reference pressure plus the constant value of Laplace pressure rise.

$$u_L n_x + v_L n_y = u_V n_x + v_V n_y = 0 \quad , \quad v_L = v_V \quad , \quad w_L = w_V \tag{6}$$

$$\left(2\mu_L \frac{\partial u_L}{\partial x} - p_L\right) n_x + \mu_L \left(\frac{\partial u_L}{\partial y} + \frac{\partial v_L}{\partial x}\right) n_y = \left(2\mu_V \frac{\partial u_V}{\partial x} - p_V\right) n_x + \mu_V \left(\frac{\partial u_V}{\partial y} + \frac{\partial u_V}{\partial x}\right) n_y$$

$$\mu_L \left(\frac{\partial u_L}{\partial y} + \frac{\partial v_L}{\partial x}\right) n_x + \left(2\mu_L \frac{\partial v_L}{\partial y} - p_L\right) n_y = \mu_V \left(\frac{\partial u_V}{\partial y} + \frac{\partial v_V}{\partial x}\right) n_x + \left(2\mu_V \frac{\partial v_V}{\partial y} - p_V\right) n_y \tag{7}$$

$$\mu_L \frac{\partial w_L}{\partial x} n_x + \mu_L \frac{\partial w_L}{\partial y} n_y = \mu_V \frac{\partial w_V}{\partial x} n_x + \mu_V \frac{\partial w_V}{\partial y} n_y$$

$$n_L D_L \frac{\partial Y_L}{\partial x} n_x + n_L D_L \frac{\partial Y_L}{\partial y} n_y = n_V D_V \frac{\partial Y_V}{\partial x} n_x + n_V D_V \frac{\partial Y_V}{\partial y} n_y \tag{8}$$

$$Y_V = \frac{Y_L}{\beta - (\beta - 1) Y_L} \tag{9}$$

Equation (9) is the equilibrium relationship for an ideal binary solution where β is the relative volatility. Subscripts '*L*' and '*V*' refer to values in the liquid and vapour phases, respectively. Finally, there are two bulk constraints that must be satisfied:

$$\frac{dP_{BL}}{dz} = \frac{dP_{BV}}{dz} \tag{10}$$

$$n_V w_{BV} A_V \frac{dY_{BV}}{dz} = -n_L w_{BL} A_L \frac{dY_{BL}}{dz}$$

$$\text{where } w_{BV} = \frac{1}{A_V} \int_{A_V} w_V dA \ , \ w_{BL} = \frac{1}{A_L} \int_{A_L} w_L dA \ , \ Y_{BV} = \frac{1}{w_{BV} A_V} \int_{A_V} w_V Y_V dA \ , \ Y_{BL} = \frac{1}{w_{BL} A_L} \int_{A_L} w_L Y_L dA \tag{11}$$

Subscript '*B*' indicates a bulk value and those involved in Eq. 11 for overall species conservation are defined above in terms of integrals over the cross-section areas (A_L, A_V) occupied by the liquid and vapour phases.

2.2 Simplified model for spiral mass transfer

The mass transfer coefficients in the vapour and liquid phases are determined from the solution to Eqs. 1-11 by:

$$k_V (Y_{BV} - Y_{VI}) = -n_V w_{BV} \frac{dY_{BV}}{dz} \frac{A_V}{H} \tag{12}$$

$$k_L (Y_{LI} - Y_{BL}) = n_L w_{BL} \frac{dY_{BL}}{dz} \frac{A_L}{H} \tag{13}$$

$$\text{where} \quad Y_{LI} = \frac{1}{L}\int_L Y_L dl \quad \text{and} \quad Y_{VI} = \frac{Y_{LI}}{\beta - (\beta - 1)Y_{LI}}$$

(L is length of the interface in the channel section.) So, with k_V and k_L known, the bulk phase compositions as a function of position s along the contacting channel can be determined by the bulk species balances for the two phases:

$$n_V w_{BV} A_V \frac{dY_V}{ds} = k_V (Y_{VI} - Y_{BV}) H \tag{14}$$

$$n_L w_{BL} A_L \frac{dY_L}{ds} = k_L (Y_{LI} - Y_{BL}) H \tag{15}$$

n_V, n_L, w_{BV} and w_{BL} are constant (developed flow with small pressure changes) and are taken from the experimental condition. The boundary conditions are the known liquid feed composition at the spiral inlet and a condition on vapour composition at the spiral outlet where vapour enters from the reboil region. Here an ideal model which assumes equilibrium between the vapour reflux and the liquid product and enforces species balance is used. The resulting boundary condition is a quadratic equation for Y_{LR}, the liquid product for the reboiler, interms of the liquid mole fraction at the spiral outlet (Y_{LS}). Solving gives the relation final boundary condition with Y_{VS} determined from the equilibrium relation Eq. 9.

$$Y_{LR} = \frac{\beta(N_L + N_V) + (\beta - 1)N_L Y_{LS} - N_V - \sqrt{[\beta(N_L + N_V) + (\beta - 1)N_L Y_{LS} - N_V]^2 - 4(\beta - 1)(N_L + N_V)\beta N_L Y_{LS}}}{2(\beta - 1)(N_L + N_V)} \tag{16}$$

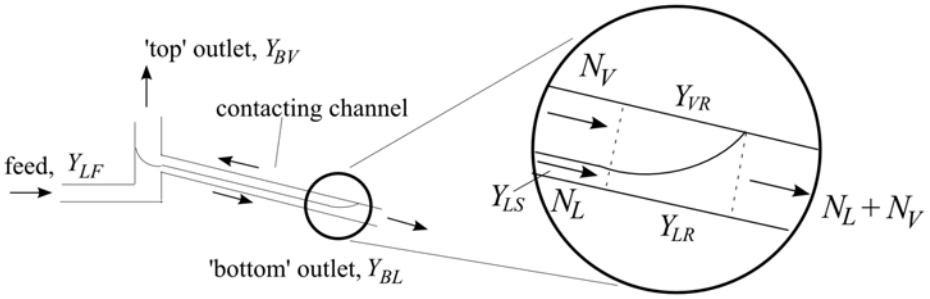

Fig. 3. Schematic diagram of the microchannel distillation process. The reboiler region is shown in inset.

The computed system corresponded to the experimental system which was 2,2-dimethylbutane (22dmb) and 2-methyl-2-butene (2m2b). The relative volatility is found to have constant value $\beta = 1.44$ within 0.5% over the full range of composition, according to values determined based on an ideal binary solution and the Antoine equation for pure component vapour pressures (Sinnott, 2005). Diffusivities for the vapour phase were calculated using the Hirschfelder-Bird-Spotz correlation and diffusivities in the liquid phase using the Wilke-Chang correlation (Treybal, R. E., 1980). Viscosities and densities in the range of temperature were estimated using ASPEN Properties 11. Average values over the range and composition are used for each phase as listed in Table 1.

Table 1. Binary components and contant property values for each phase used in the computations.

Component	Formula	BP ^oC, 1 atm
2m2b	C5H10	38.56
22dmb	C6H14	49.74

Phase	Density, kg/m^3	Viscosity, Pa s	Diffusivity, m^2/s
Liquid	631	2.27×10^{-4}	4.9×10^{-9}
Vapour	3.00	7.45×10^{-6}	3.5×10^{-6}

3. RESULTS

Computational prediction is now made using Eqs. 1-16 for the experimental condition. The measured flow rates uniquely determine the fraction of area occupied by each phase in the flow section and the value of bulk pressure gradient. dP_B/dz = 12.8 kPa/m and $A_L/(A_L + A_V)$ = 0.113 in the computation reproduce the experimental flow rates of 93.9 μg/s and 104 μg/s for the vapour and liquid phases, respectively. This fixes the flow field and solution of the species equation for appropriate reference values and bulk gradients then generates results for the phase mass transfer coefficients, k_L and k_V, as functions of the bulk compositions in the phases. An example computational result is shown in Fig. 4. It was found that the mass transfer coefficients were weakly dependent on the bulk gradients and could be expressed accurately as functions of a single parameter representing average level of mole fraction, $Y_{avg} = (Y_{BL}+Y_{BV})/2$. The computed values of k_L and k_V for dY_{BL}/dz = 5 (which is found to be near the experimental conditions) as a function of Yave is shown in Fig. 5 along with the polynomial functions that fit the results.

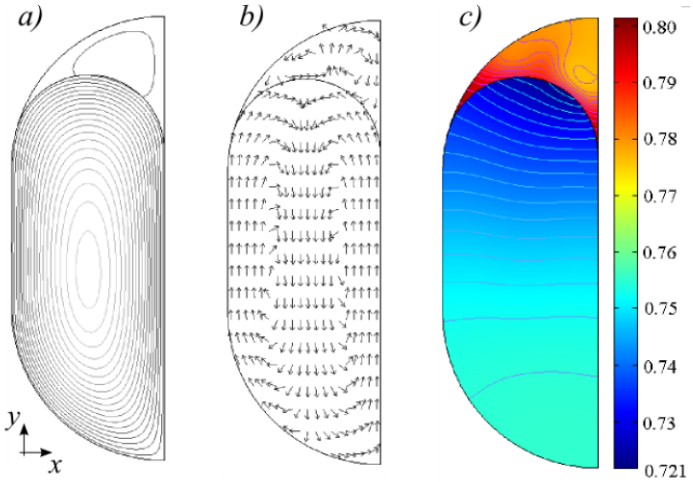

Fig. 4. a) Streamwise velocity contours (w_{max}=0.0445 m/s, w_{min}= -2.246 m/s) b) Secondary motions produced by the Coriolis force (arrows show direction but not magnitude) c) mole fraction contours.

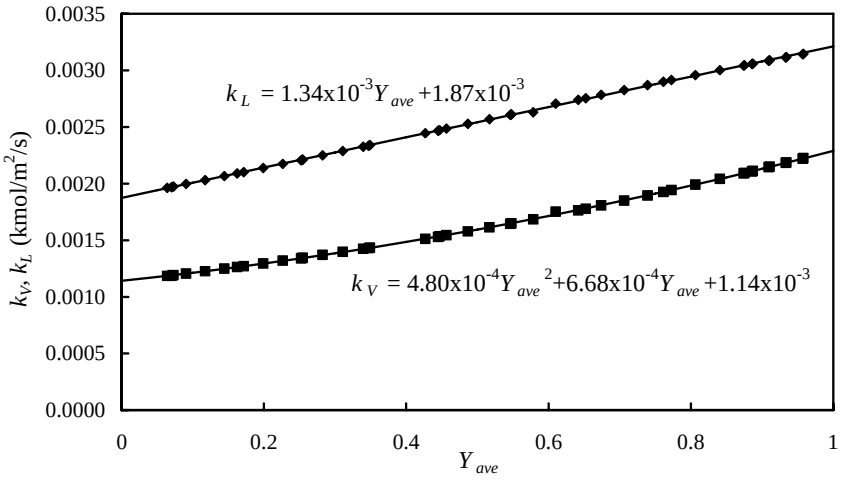

Fig. 5. Computed results for k_L and k_V (dY_{BL}/dz = 5); polynomial fitting functions (rms error, 0.2%).

With the fitting functions for mass transfer coefficients, Eqs. 14-16 are solved to determine bulk phase mole fractions along the contacting channel for the experimental condition. The experimental channel length is 6.88 cm

up to the point where temperature reaches the boiling point of the heavy-component (22dmb) and this is assumed to be the contacting channel length for the solution. The results for computed bulk mole fractions are plotted in Fig. 6 where the level computed for the liquid product stream from the reboil region is also indicated. The final computed conditions for outlet stream mole fractions are compared with the values measured in Table 2. Clearly, for both the mole fraction of the enriched liquid product (Y_{LR}) and that of the vapour outlet stream (Y_{BV} at $s = 0$), the agreement to within 1.1% of the measured values is excellent. The computational approach thus appears to have considerable promise for aiding development of rotating spiral contacting technology.

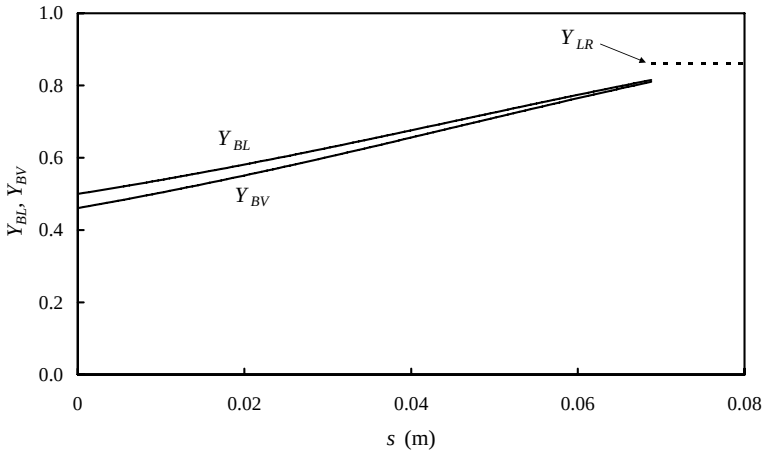

Fig. 6. Computed bulk mole fraction of heavy component (22dmb) in each phase along the spiral channel.

Table 2. Comparison between experimental and computed results.

	Experimental	Computed	Difference
Y_{LR}	0.870	0.860	1.1%
Y_{BV} ($s = 0$)	0.464	0.461	0.6%

4. CONCLUSIONS

A numerical computation of flow and mass transfer was carried out for an experimental case of rotating spiral microchannel distillation. The mass transfer coefficients for the liquid and vapour phases were determined computationally and these were used to predict measured compositions. The computation results agreed with those measured to within 1.1%. Therefore it appears likely that the computational approach can play an important role in future development of devices based on rotating spiral phase contacting.

5. REFERENCES

MacInnes, J. M., Priestman, G. and Allen, R. W. K., (2005). A spinning microchannel multiphase contactor. Proceedings of the 2005. World Congress of Chemical Engineering. Glasgow, UK.

MacInnes, J. M., Ortiz-Osorio, J., Jordan, P., Priestman, G., and Allen, R. W. K. (2008). Demonstration of rotating spiral microchannel distillation. Submitted for publication.

Sinnott, R. K., (2005) Coulson and Richardson's Chemical Engineering Series: Chemical Engineering Design. Fourth edition. Volume 6. pp 936-958 Butterworth-Heinemann.

Tonkovich, A., Jarosh, K., Arora, R., Silva, L., Perry, S., McDaniel, J., Daly, F., and Litt, B. (2008). Methanol production FPSO plant concept using multiple microchannels unit operations. Chemical Engineering Journal 135S. s2-S8.

Tonkovich, A., Simmons, W., Silva, L., Qiu, D., Perry, S., and Yuschak, T. (2007). Distillation process using microchannel technology, US Patent no. 7,305,850.

Treybal, R. E., (1980) Mass Transfer Operations. Third Edition. McGrawHill.

Wootton, R. and deMello, A. (2004). Continuous laminar evaporation: micron-scale distillation, Chemical Communications 2. 266-267.